Paper pa02-068
Submitted to the 28th International Conference on High Energy Physics
ICHEP'96, Warsaw, Poland, July 1996

Thrust Jet Analysis of Deep–Inelastic Large Rapidity Gap Events at HERA

H1 Collaboration

Abstract

Large Rapidity Gap events in deep inelastic ep collisions, observed with the H1 detector at HERA, have been subjected to a thrust jet analysis. The analysis is based on the 1994 data and corresponds to an integrated luminosity of $1.96\,\mathrm{pb}^{-1}$. The average event thrust is analysed in intervals of the hadronic mass M_X which ranges from $6-36$ GeV^2 and the dependence on Q^2 and P_t^2, the thrust jet transverse momentum, are investigated. Comparison with e^+e^- data shows that the average thrust in large rapidity gap events is significantly smaller. The P_t^2 distributions of the thrust jets, covering the interval $[0-140]$ GeV^2, show that although most of the events have the thrust axis aligned with the γ^*p collision axis, a substantial high P_t tail is present. These P_t^2 distributions are almost independent of M_X. The large P_t behaviour observed in the data cannot be explained in terms of a simple Aligned Jet Model for diffractive deep-inelastic scattering and the inclusion of substantial hard gluon radiation is needed.

1 Introduction

Measurements at HERA have since 1992 established the existence of a class of events, called large rapidity gap events, which have no hadronic energy flow in a pseudo rapidity interval adjacent to the proton direction [1, 2]. These events are consistent with, and can be interpreted as, a diffractive virtual boson proton interaction i.e resulting from pomeron ($I\!P$) exchange [3, 4]. However, as to the mechanism which leads to these events at the parton level, substantial unknowns still exist which have resulted in the development of different rapidity gap models [5, 6].

In the present paper we will investigate final state properties of the large rapidity gap events using a thrust jet analysis. Because of the large HERA energy, the photon can dissociate into a system X (see Fig.1) of hadrons with large invariant mass M_X of up to 40 GeV and more, together with low momentum transfers to the proton ($|t| < 1$ GeV^2), leaving the proton intact. The range in mass M_X is appropriate for an analysis of the topological characteristics of X in terms of the variable thrust, much as was used in e^+e^- interactions in the same $\sqrt{s}$ range. Further, the existence of the rapidity gap adjacent to the proton direction means that the final state is fully measured.

The thrust analysis method used here exploits the event characteristics intrinsic to a "2-jet" topology. It provides a powerful tool to investigate the overall event properties of all events in the M_X range considered. For example, the event thrust value is sensitive to the higher order parton diagrams in pQCD, and the transverse momentum P_t of the thrust jet with respect to the $\gamma^* p$ collision axis is a measure of the p_t of the underlying leading order partonic subprocess.

The simplest partonic picture for diffractive virtual photon dissociation into hadrons is the Aligned Jet Model (AJM) proposed by Bjorken [7] in which the photon fluctuates into a longitudinally very asymmetric $q\bar{q}$ system allowing for small intrinsic k_t only, as a result of "colour transparency" [8]. In addition two approaches to the parton level of large rapidity gap event production that include hard gluon radiation have been modelled for comparison with the data. One approach [9] is based on deep inelastic scattering off a pomeron or reggeon emitted by the proton, whereas the other one [10] is based on usual deep inelastic ep scattering with an additional soft colour interaction [5, 6] leading to X and Y (Fig.1) as colour singlet states.

2 Thrust Jet Analysis Method

In the center of mass of a system X of N particles, the thrust method determines the direction $\vec{a}$ along which the projected energy flow is maximal. Thrust is computed as:

$$T = 1/M_X \cdot \max_{\vec{a}} \sum_{i=1}^{N} |\vec{p}_i . \vec{a}|$$

where $\vec{p}_i$ represents the momentum of particle i and M_X is the invariant mass of the system X. Given the axis $\vec{a}$, the particles can then be uniquely grouped into two subsets (*thrust jets*), depending on whether their momentum component along the thrust axis is positive or negative. The 4-momentum vectors of the two thrust jets have independent masses, and opposite but equal size 3-momentum vectors P_J. Thrust, T, is then related to the jet momenta, P_J, their masses m_i and M_X by:

$$T^2 = (2 * P_J/M_X)^2 = 1 - 2 \cdot \frac{m_1^2 + m_2^2}{M_X^2} + \frac{(m_1^2 - m_2^2)^2}{M_X^4}.$$

Thrust values range from a maximum value of $T = 1$, in the case of a two particle state, to a minimum value of $T = 0.5$, obtained in isotropic events with an infinite multiplicity. A symmetric 3 particle configuration yields a value $T = 2/3$ while for a non-symmetric topology the thrust value increases and the thrust axis is aligned in the direction of the most energetic particle. Such an asymmetric 3 particle topology then appears in a 2 jet-like configuration with a thrust value $T \geq 2/3$.

If an event has an underlying partonic subprocess, the two back-to-back reconstructed thrust jets are correlated with the hard partons. In the case of a two massless parton configuration, the thrust value at the parton level is $T_{pa} = 1$, and will be reduced at the hadron level to a value $T_{had} = P_J/P_{pa}$. The direction of the thrust axis at the hadron level remains, within resolution, aligned to the direction of the 2 (back-to-back) partons. For an underlying 3 parton system, the direction of the reconstructed thrust axis at the hadron level is aligned with the direction of the most energetic parton. This correlation property has been verified for events, generated as $q\bar{q}g$ events using the RAPGAP event generator [9], for final states with masses $M_X \gtrsim 5$ GeV . Hadronisation and detector simulation were included in the event reconstruction. Hence, even in 3-parton events, where the three jets cannot yet be resolved at the hadron level, the thrust axis will identify the parton with the largest momentum, but the parton momentum value is reduced.

The transverse jet momentum, P_t, is defined as the *thrust jet* momentum transverse to the proton beam direction as seen in the overall centre of mass of the system X. This direction is the best approximation to the true $\gamma^* I\!\!P$ axis in the experiment, as the direction of $I\!\!P$ is not measured and the direction of γ^* is subject to measurement resolution.

3 Detector Description and Event Selection

In the following, only the detector components relevant for this analysis are reviewed. A detailed description of the H1 detector can be found elsewhere [11].

The "backward" electromagnetic calorimeter (BEMC), extending over a polar angular range of $151^\circ < \theta < 176^\circ$ with full azimuthal coverage, was used to trigger and measure the energy of the scattered electron in the DIS processes. The BEMC electromagnetic energy resolution is $\sigma_E/E = 0.10/\sqrt{E\ [\mathrm{GeV}]} \oplus 0.42/E[\mathrm{GeV}] \oplus 0.03$ [11], while the absolute electromagnetic energy scale is known with an accuracy of 1.0%. The BEMC hadronic energy scale is only known to a precision of 15%. The backward proportional chamber (BPC) located in front of the BEMC detector has an angular acceptance of $155.5^\circ < \theta < 174.5^\circ$ and measures in conjunction with the interaction vertex, the direction of the scattered electron with a precision of 1 mrad. These "backward" detectors accept DIS processes with Q^2 values ranging from 5 to 120 GeV^2 . The LAr calorimeter extends over the polar angular range $15^\circ < \theta < 165^\circ$ with full azimuthal coverage. The electromagnetic energy resolution is $\sigma_E/E \approx 0.12/\sqrt{E\ [\mathrm{GeV}]} \oplus 0.01$, while the hadronic energy resolution is $\sigma_E/E \approx 0.50/\sqrt{E\ [\mathrm{GeV}]} \oplus 0.02$. A study of the transverse momentum balance between the positron and the hadronic final state has shown that the absolute hadronic energy scale is known to an accuracy of 4%. The LAr calorimeter is surrounded by a superconducting solenoid providing a uniform magnetic field of 1.15 T parallel to the beam axis in the tracking region. The track reconstruction is essentially based on the information from the central jet chamber (CJC) and the z-drift chambers. These detectors cover a polar angular range of $15^\circ < \theta < 165^\circ$ and provide, with a maximum of 56 points per track, a good momentum reconstruction ($\delta p_t/p_t \leq 0.01\ p_t$).

Apart from the LAr calorimeter, which covers the rapidity range up to $\eta \approx 3.7$, the following detectors have been used in the definition of the event rapidity gap:

- the plug calorimeter, a copper/silicon calorimeter;
- the forward muon spectrometer which complements the muon identification in the forward direction. It also detects particles resulting from secondary interactions in the beampipe and in adjacent material depositing energy;
- the forward proton tagger, a lead/scintillator sandwich calorimeter, located 24 m from the interaction point;

These detectors extend the pseudo rapidity range to a value of 7.5. In order to minimize model dependencies, the hadronic final state of each event is decomposed in two subsytems X and Y (fig. 1), separated by the largest rapidity gap in the event. For diffractive events, M_X and M_Y are requested to be much smaller than the total hadronic invariant mass W of the system.

In the present analysis, the standard DIS variables x_{BJ}, y_e and Q^2 were calculated from the measured electron parameters:

$$Q^2 = 4E_eE_{e'}\cos^2(\tfrac{\Theta_e}{2}) \qquad y_e = 1 - \tfrac{E_e}{E_{e'}}\sin^2(\tfrac{\Theta_e'}{2}) \qquad x_{BJ} = \tfrac{Q^2}{y_e s}$$

where E_e and $E_{e'}$ are the energy of respectively the incident electron and the scattered electron and $\Theta_{e'}$ is the electron scattering angle. The invariant mass M_X of the diffractive hadronic system, excluding the colourless proton remnant Y, is calculated as :

$$M_X^2 = (E_{e'} - P_{z_{e'}})(E_h + P_{z_h}) - \textstyle\sum_{hadr}(P_{x_i}^2 + P_{y_i}^2)$$

where

$$E_h = \textstyle\sum_{hadr} E_i \qquad P_{z_h} = \textstyle\sum_{hadr} P_{z_i}$$

and E_i, P_{x_i}, P_{y_i}, P_{z_i} are the energy and momentum components of the final state hadron i, calculated from tracks and calorimeter clusters (see section 4). Using $E_{e'} - P_{z_{e'}}$ from the electron measurement in the expression for M_X leads to a better reconstruction as it is not affected by losses of hadrons in the backward direction. From the previous quantities two further variables β and $x_{I\!P}$ can be calculated :

$$\beta = \tfrac{Q^2}{Q^2+M_x^2}, \qquad x_{I\!P} = \tfrac{Q^2+M_x^2}{Q^2}\cdot x.$$

In the "proton infinite momentum frame", the variable $x_{I\!P}$ can be interpreted as the momentum fraction carried by the interacting $I\!P$, while β is the momentum fraction of the $I\!P$ carried by the parton interacting with the photon. In the above formulae the 4-momentum transfer squared between the incident proton and the final state colourless proton remnant, Y, has been neglected ($|t| \ll Q^2$).

The DIS event sample used in this analysis was obtained from the data collected during the 1994 HERA running, corresponding to an integrated luminosity of $1.96\,\mathrm{pb}^{-1}$. The basic event trigger required a minimum energy deposition in the BEMC ($E_e \geq 4$GeV). The sample was subjected to the following event selection criteria :

1. the scattered electron energy was constrained to $y_e < 0.5$ while the scattering angle was limited to $156° < \theta_e < 173°$
2. a rapidity gap was imposed, by requiring $\mathrm{E_{Plug}} < 3$ GeV , the number of track segments in the forward muon tracker ≤ 1, no hit in the proton tagger and no energy deposition (E < 0.4 GeV) in the LAr calorimeter for $\eta > 3.2$ ("η_{max} cut") and $x_{I\!P} < 0.05$;
3. the z position of the interaction vertex reconstructed with at least 1 good CJC track, was constrained to the interval -25 cm $\leq z \leq 35$ cm;
4. for a valid thrust analysis, at least 3 particles (charged or neutrals) in addition to the electron were required; the invariant mass of the hadronic final state was also requested to be bigger than 4 GeV.

The data distributions are fully corrected for detector resolution and acceptances to the kinematic range $M_Y < 1.6$ GeV , $x_{I\!P} < 0.05$, $10 < Q^2 < 100$ GeV/c^2 and $y < 0.5$. The M_Y limit ensures that the system Y is a leading system carrying more than 95% of the incident proton momentum. Under such circumstances a large rapidity gap must always occur from kinematic considerations alone. The breakdown of the selected events in the 7 mass intervals used for the thrust analysis, covering the mass range from 4 GeV to 36 GeV, is shown in Table 1.

	M_X intervals (GeV)						
	4-6	6-8	8-11	11-15	15-19	19-24	24-36
observed	1439	1278	1404	1130	711	502	401

Table 1: Number of uncorrected events per M_X bin

The range and mean values for the parameters Q^2, x_{BJ}, $x_{I\!P}$ and W, averaged over the full mass range 4 GeV $\leq M_X \leq 36$ GeV , are shown in Table 2 .

4 Final State Reconstruction, Unsmearing and Acceptance Corrections

Hadronic final states with all particle energies above 2 GeV can be well reconstructed using the calorimetric information only. However, for particles at lower energies, due to

Parameter	Range	Mean value
Q^2	(5 - 100) GeV ^{2}	22 GeV ^{2}
x_{Bj}	10^{-4} - $3.2 \cdot 10^{-2}$	$2 \cdot 10^{-3}$
$x_{\mathbb{P}}$	10^{-4} - $5 \cdot 10^{-2}$	0.014
W	30 - 210 GeV	136 GeV

Table 2: Event sample characteristics for 4 GeV $\leq M_X \leq 36$ GeV

sampling fluctuations, calorimeter cracks and the application of a calorimeter noise cut, a fraction of the particle energy can be lost, resulting in an incomplete description of the final state. In order to compensate for this loss and to avoid track-cluster matching schemes, the following scheme was used. Every reconstructed track is, in addition to the clusters, added to the list of final state momentum vectors, but the track momentum is bounded by a momentum limit P_{lim}. On the average P_{lim} compensates for the undetected energy in the calorimeter. Optimisation of the transverse momentum balance between the scattered electron ($p_t^{e_{scat}}$) and the hadronic final state (p_t^{had}) yields a value $P_{lim} = 350$ MeV $/c$. With this addition of the track information in the final state recontruction, the distribution $p_t^{had}/p_t^{e_{scat}}$ becomes narrower than the one obtained from clusters only, and has a mean value of 1.00 ± 0.01, both in data and in simulated events.

Two Monte Carlo simulations are used here to unfold the observed experimental distribution for acceptance and detector smearing effects. The simulated events are tuned, to reproduce the P_t and thrust distributions of the data. All known detector effects are included in the event simulation, and the events are processed through the standard H1 reconstruction programs. It is found that the resolution of the thrust jet P_t is approximately 1 GeV $/c$.

The experimental P_t^2 and thrust distributions are unfolded on a bin by bin basis. In the case of the P_t distributions, the correction factors vary only moderately from bin to bin and are large (> 2) only for masses $M_X > 15$ GeV and for $P_t^2 < 1$ (GeV $/c)^2$. For the thrust distributions the correction factors become important for masses $M_X > 15$ GeV and thrust values $T > 0.85$.

To estimate the systematic errors, the following contributions are taken into account:

- uncertainty in the LAr hadronic energy scale ($\pm 4\%$);
- uncertainty in the BEMC hadronic scale ($\pm 15\%$);
- uncertainty in the correction factors due to parameter tuning and different hadronisation schemes used in the event simulation.

No additional systematic uncertainty was included to account for uncertainties of the reconstruction procedure of the hadronic final state, in view of the good description of the event multiplicity distribution and overall event p_t balance.

The statistical and systematic errors are indicated on the figures as the inner and outer error bars respectively.

5 Monte Carlo Models

Two different models are used to simulate large rapidity gap events. The first model, labelled RG, is based on the RAPGAP generator [9]. The basic mechanism assumed there follows the idea of Ingelman and Schlein [12] in which a flux of pomerons can be associated with the proton. The partonic subprocesses that are considered are shown by the diagrams in Fig. 2.

The simplest model, hereafter labeled as $q\bar{q}$, only uses the subprocess of diagram 2a, in which no intrinsic P_t of the quarks with respect to the $I\!P$ direction is assumed, and the virtuality of the quark mediating the interaction between the photon and the pomeron is the smallest kinematically allowed. This model is taken as an approximation for the AJM, in which one quark of the $q\bar{q}$ pair which couples to the photon and interacts with the proton in a way which is characteristic for soft hadron processes i.e. low p_t. The $\beta_q = x_{q/I\!P}$ distribution is assumed to be flat.

For the model labeled RG both the Compton QCD and Boson Gluon Fusion diagrams are taken into account. However, if the transverse momentum in the hard process ($\hat{p}_t$) falls below a cutoff value of 2 GeV/c, the $q\bar{q}$ process is used instead. The RG model uses the parton densities obtained from a QCD analysis of the diffractive structure function [13], from the 1994 data, using DGLAP evolution. The input parton density distribution at the ${Q_0}^2$ (${Q_0}^2 = 2.5$ (GeV/c)^2) of the evolution scale is dominated by gluons carrying most of the fractional momentum ($x_{g/I\!P}$).

In all these simulations, higher order gluon emission is taken care of by the parton shower mechanism and the hadronisation by the Lund string fragmentation model. In particular for the $q\bar{q}$ model these mechanisms produce p_t well in excess of those expected in the AJM.

The second model, labeled SCI, is based on the event generator LEPTO6.4 [10]. Here rapidity gap events are generated as standard ep DIS events using the proton structure function and hard scattering processes, complemented by non-perturbative soft color interactions. This addition can convert the hadronic final state and proton remnant into a colour singlet state such that at hadronisation large rapidity gaps occur.

Apart from the conceptual model differences which exist between the RG and the SCI models it should also be emphasised that the handling of the $\hat{p}_t$ cutoff in both programs is different.

6 Results

Fig. 3a shows the average thrust $< T >$ for 7 mass intervals M_X. Taking a thrust value of 2/3 as a reference for an isotropic 3-jet configuration, one observes first of all that for all masses the thrust $< T >$ is always larger than 2/3, and furthermore that the event thrust increases with M_X. These two features indicate a growing back to back correlation in the energy flow, representing the hadronic final state topologically as an elongated 2-jet pattern. The increase of the average thrust with M_X indicates, given that the particle multiplicity also increases with M_X, that the computed thrust direction represents a real topological axis for the event. A similar evolution of $< T >$ with M_X is observed in e^+e^-

annihilation [14] for data covering a comparable invariant mass range (Fig. 3a). In all mass intervals, the average thrust for the large rapidity gap events is significantly smaller than in e^+e^- annihilation, by an amount $\Delta T \sim 0.07$.

Fig. 3a also shows the thrust dependence on M_X for two subclasses of events, with respectively $P_t < 1$ GeV/c and $P_t > 1$ GeV/c. For a given mass interval, the average thrust value in the high P_t event sample is significantly lower than the thrust value in the low P_t event sample. The difference is about 0.04 over the complete mass range, indicating that for a given mass M_X, events with a larger P_t are less 2-jet like.

To investigate the dependence of thrust on Q^2, the events were distributed into two classes containing events with $10 < Q^2 < 20$ GeV^2 and $30 < Q^2 < 100$ GeV^2 respectively. No clear Q^2 dependence could be observed within the resolution of $\sigma_T \sim 0.01$

Predictions for the average thrust values as obtained from the two different models RG and SCI are shown in Fig. 3b. The $q\bar{q}$ model (not shown) gives a much too elongated final state. The results from the soft color interaction model approximates best the data. The thrust prediction from the RG model is too high. The RG prediction for $< T >$ can be lowered by choosing a lower $\hat{p}_t$ cutoff. An optimization of the $\hat{p}_t$ cutoff has not been attempted. In the LEPTO program a different $\hat{p}_t$ cutoff scheme is used. The observed differences in $< T >$ for the event samples with $P_t < 1$ GeV $/c$ and $P_t > 1$GeV/c are fairly well reproduced by both models.

Normalised P_t^2 distributions, for 6 M_X intervals covering the mass range from 6 to 36 GeV, are shown in fig. 4a. Only those P_t^2 intervals are shown in which all events have a $P_{t,max}$ ($P_{t,max} = (M_X/2) \cdot T$) value exceeding the P_t^2 upper bin limit. A very striking feature of the P_t^2 distributions is that they are dominated by small P_t values, which are far below the allowed kinematical $P_{t_{max}}$ limit. Equally striking is that these P_t^2 distributions show no dependence on the final state mass M_X. Although the event fractions over the full P_t^2 interval vary by a factor 1000, the P_t^2 distributions in the different mass intervals coincide to within 20%, indicating that, within statistical errors the production cross section factorises and can be written as

$$1/\sigma \cdot \mathrm{d}\sigma/\mathrm{d}P_t^2(M_X, P_t^2) = A(M_X) \cdot G(P_t^2).$$

The mass independent P_t^2 distribution varies with P_t, between approximate behaviours $G(P_t^2) \propto P_t^{-2}$ for $P_t^2 \sim 1\,(\mathrm{GeV/c})^2$ and $G(P_t^2) \propto P_t^{-4}$ for $P_t^2 > 10\,(\mathrm{GeV/c})^2$.

To exhibit the features born out by the data, the normalised P_t^2 distribution in the mass range $19 < M_X < 24$ GeV is displayed in Fig. 4b on a linear scale. The data clearly show

1. a steep rise of the distribution towards low P_t values, indicating an alignment of the final state thrust axis with the initial $\gamma^* p$ collision direction.

2. a substantial large P_t^2 tail up to 80 $(\mathrm{GeV/c})^2$.

The prediction of the $q\bar{q}$ model, in which no hard gluon radiation or large virtuality is present but which includes parton showers and fragmentation, cannot account for the observed large P_t^2 tail. In contrast, the 2 models RG and SCI which also include the boson gluon fusion and the QCD Compton diagrams, qualitatively reproduce the large P_t^2 tail.

The fraction of events with P_t^2 values above 1.0 (GeV/c)^2 and 3.0 (GeV/c)^2 for 6 M_X values is shown in Fig. 5. The observed rise with M_X at lower M_X mainly reflects the extension of P_t^2 kinematic range. Towards higher masses the fraction rises less, reaching large values of 64% for $P_t^2 > 1$ (GeV/c)^2 and 38% for $P_t^2 > 3$ (GeV/c)^2. None of the models describes the data well. The RG model predicts event fractions significantly below the data. The SCI model leads to a fair agreement with the data above 1 (GeV/c)^2, but also fails to predict event fractions at $P_t^2 > 3$(GeV/c)^2. The result of the $q\bar{q}$ simulation (not shown) is far below the data, at a level of about 1/3.

7 Discussion and Conclusions

The thrust analysis has revealed the following topological properties of the large rapidity gap events :

1. they show a 2-jet like configuration which gets more pronounced with M_X growing;
2. they show a 2-jet like configuration which becomes less pronounced with increasing P_t;
3. the majority of the events have limited P_t values indicating an alignment of the thrust axis with the initial state $\gamma^* p$ direction;
4. more than half of the events have P_t values larger than 1 GeV, i.e. larger than expected for soft processes;
5. the shape of the P_t distributions is independent of M_X.

These features together provide clear evidence for an underlying parton structure with a strong directional correlation to the $\gamma^* p$ axis. Feature (2), however, cannot be understood in terms of a 2-parton ($q\bar{q}$) configuration only. The events with larger P_t cannot be attributed to a $q\bar{q}$ system with larger intrinsic k_t which would not change thrust. Also the fact, that T is clearly smaller than in e^+e^- annihilation is evidence against a $q\bar{q}$ model without hard gluon radiation. Hence, we are led to conclude in a model independent way that a substantial fraction of the large rapidity gap events must contain at least one energetic gluon.

These findings imply that the simple Aligned Jet Model without gluon radiation is insufficient to explain the topology of large rapidity gap events.

All the observed features are qualitatively expected for a $q\bar{q}g$ configuration, and may be quantitatively compatible with a combination of $q\bar{q}$ and $q\bar{q}g$ events, whether they are produced via a diffractive dissociation of the virtual photon off the proton, as in the RAPGAP event simulation program, or whether they emerge from a 'normal' deep inelastic ep scattering followed by a soft colour interaction, as in the LEPTO program.

This conclusion is qualitatively sustained by the predictions of the RAPGAP Monte Carlo in which the partonic structure of the pomeron is dominated by hard gluons, as obtained from a QCD-DGLAP analysis of the diffractive structure function [13, 15], and where the BGF diagram plays an important role at the level of the hard processes.

8 Acknowledgements

We are grateful to the HERA machine group whose outstanding efforts have made and continue to make this experiment possible. We thank the engineers and technicians for their work in constructing and now maintaining the H1 detector, our funding agencies for financial support, the DESY technical staff for continual assistance, and the DESY directorate for the hospitality which they extend to the non-DESY members of the collaboration.

References

[1] ZEUS Collab., M. Derrick et al., Phys. Lett. B315 (1993) 481.

[2] H1 Collab., T. Ahmed et al., Nucl. Phys. B429 (1994) 477.

[3] H1 Collab., T. Ahmed et al., Phys. Lett. B348 (1995) 681.

[4] M. Derrick et al., Z. Phys. C 68 (1995) 569.

[5] W. Buchmüller, A. Hebecker, Phys. Lett. B355 (1995) 573.

[6] A. Edin, G. Ingelman, and J. Rathsman, Phys. Lett. B366 (1996) 371.

[7] J.D. Bjorken and J.B. Kogut, Phys. Rev. D8 (1973) 1341.

[8] V. Gribov, Sov.Phys.JETP 30 (1970) 709.

[9] H. Jung, Comp. Phys. Comm. 86 (1995) 147., Modelling Diffractive Processes, Topical Conference on Hard Diffractive Processes, Eilat, Israel, Febr.18-23 (1996) 406.

[10] G. Ingelman, A. Edin, and J. Rathsman, LEPTO 6.5 - A Monte Carlo Generator for Deep Inelastic Lepton-Nucleon Scattering, DESY 96-057.

[11] I. Abt et al., The H1 Detector at HERA, Internal Report DESY H1-96–01, to be published in Nucl. Instr. and Meth.

[12] G. Ingelman and P.E. Schlein, Phys. Lett. B 152 (1985) 256.

[13] A. Mehta, New Results on Diffractive Deep Inelastic Scattering, Topical Conference on Hard Diffractive Processes, Eilat, Israel, Febr.18-23 (1996) 710.

[14] PLUTO Collab., Ch. Berger et al., Z. Phys. C12 (1982) 297.

[15] M. Derrick et al., Z. Phys. C70 (1996) 391.

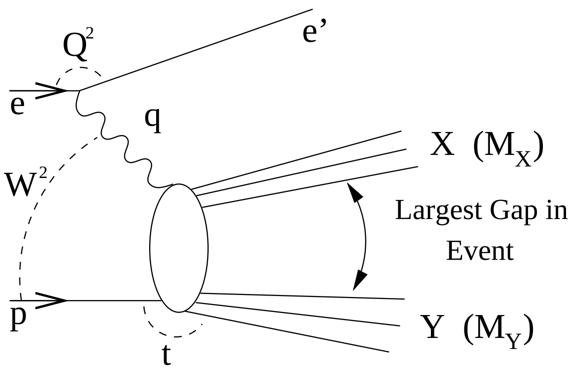

Figure 1: Definition of a rapidity gap event

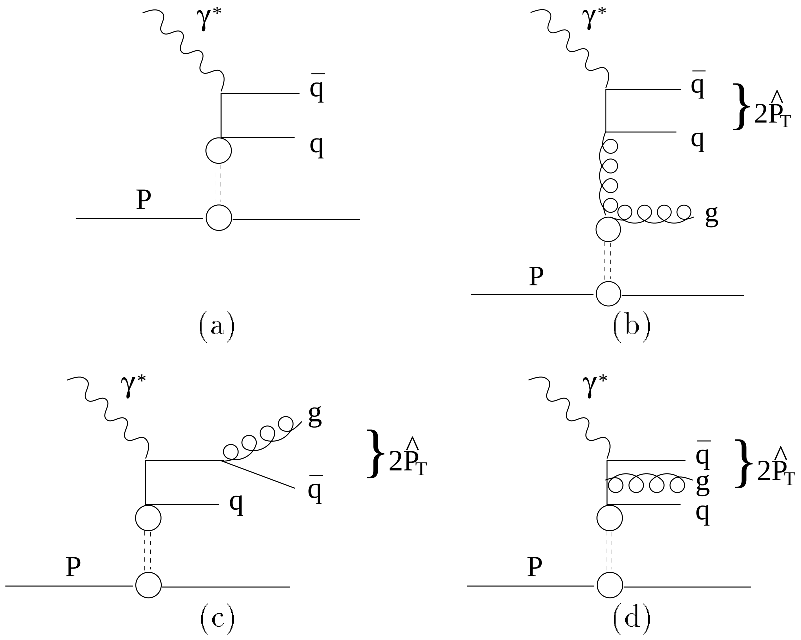

Figure 2: Diagrams for LRG events

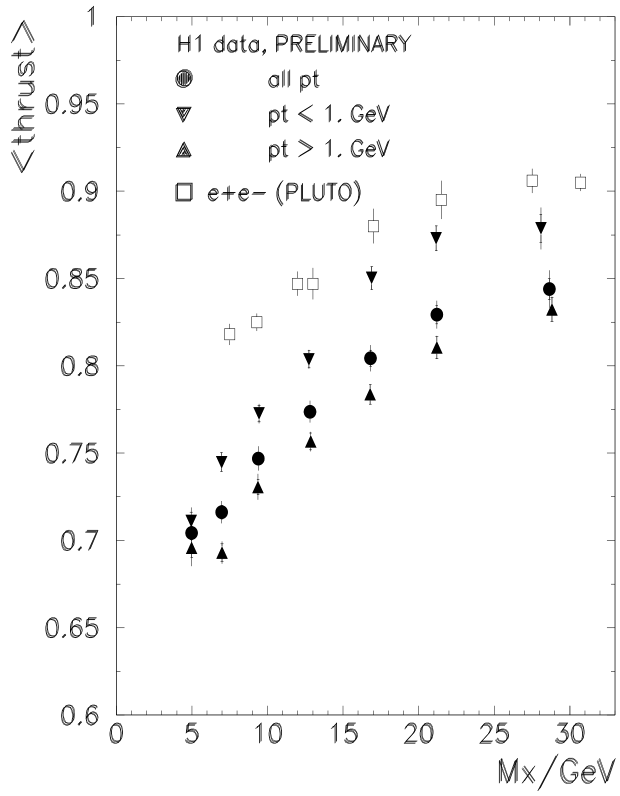

Figure 3a: Average thrust value, $< T >$ as function of the hadronic mass M_X, for all events, for events with $P_t < 1$ and events with $P_t > 1$ GeV/c; the open squares represent e^+e^- annihilation data.

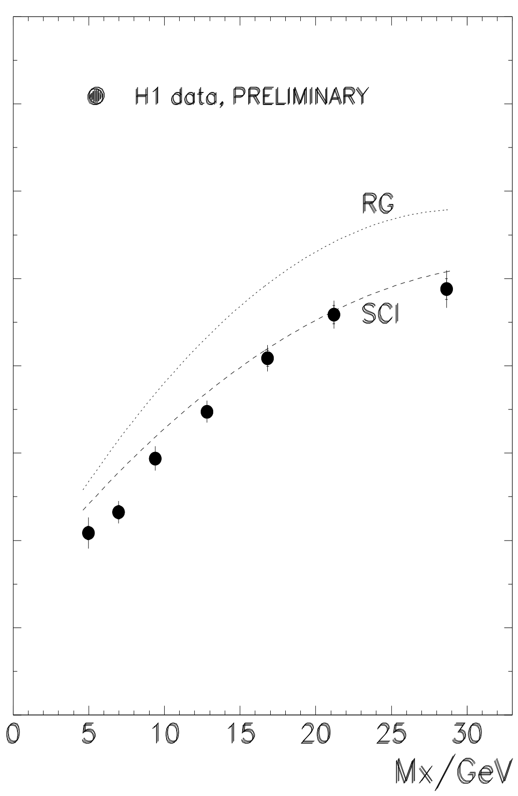

Figure 3b: Model prediction for thrust: the RG model (dotted), and the SCI model (dashed)

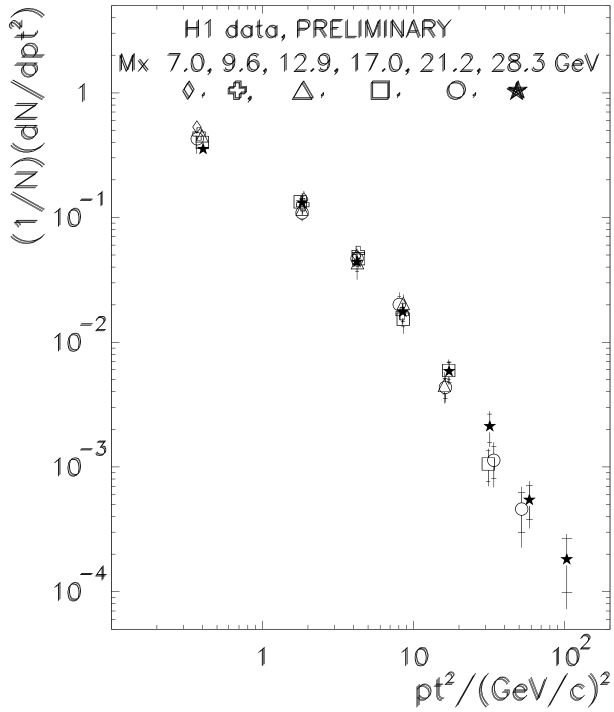

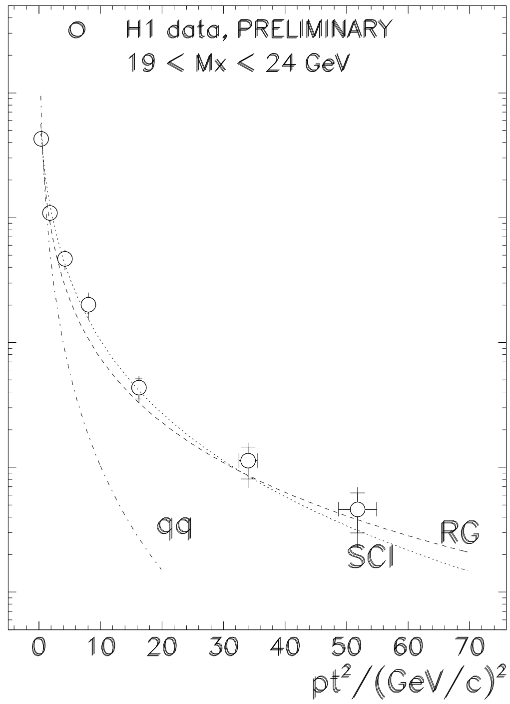

Figure 4a: Normalised thrust jet P_t^2 distributions for 6 M_X intervals. The P_t^2 intervals are 0.0, 1., 3., 6., 12., 25., 43., 79., and 151. (GeV/c)^2.

Figure 4b: Normalised thrust jet P_t^2 distributions for $19 < M_X < 24$ GeV. The curves represent the 3 model predictions (see text)

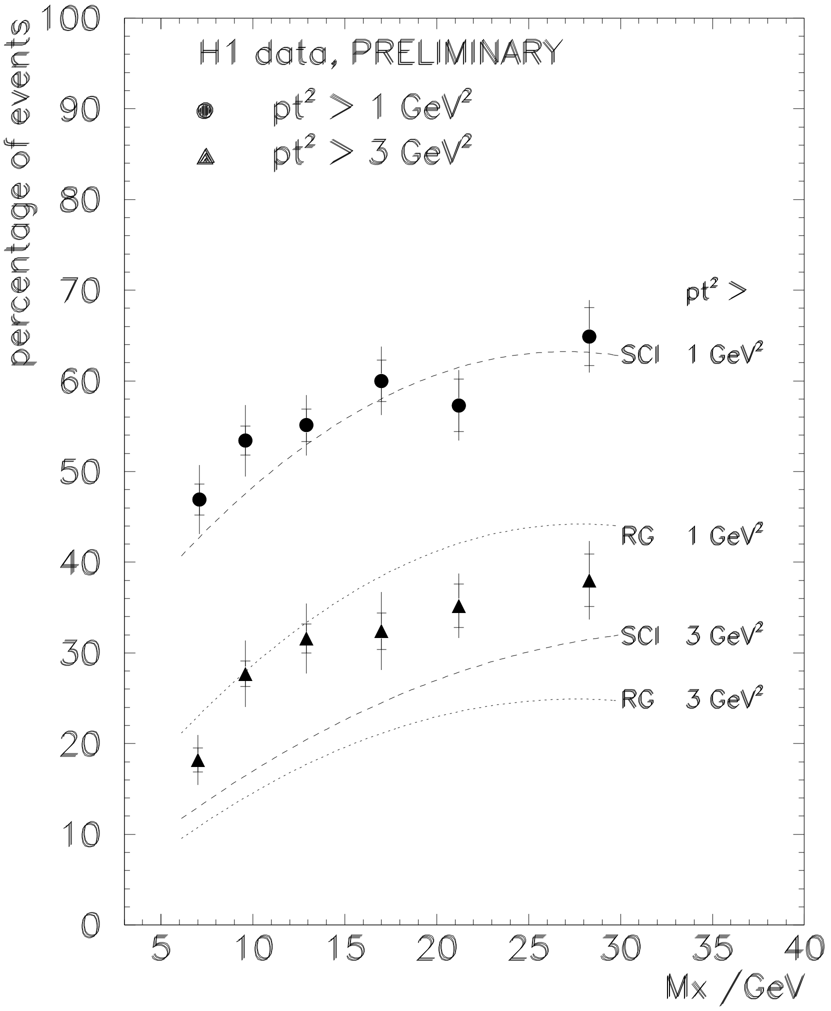

Figure 5: Fraction of events with $P_t^2 > 1(3)$ $(\mathrm{GeV/c})^2$ for 6 M_X intervals